Materials Research Bulletin 94 (2017) 472–482

Contents lists available at ScienceDirect

Materials Research Bulletin

journal homepage: www.elsevier.com/locate/matresbu

Weak ferromagnetism and superparamagnetic clusters coexistence in $YFe_{1-x}Co_xO_3$ ($0 \leq x \leq 1$) perovskites

Fernando Pomiro[a], Diego M. Gil[b,1], Vivian Nassif[c], Andrea Paesano Jr.[d], María I. Gómez[e], Julio Guimpel[f,1], Rodolfo D. Sánchez[f,*,1], Raúl E. Carbonio[a,*,1]

[a] INFIQC (CONICET – Universidad Nacional de Córdoba), Departamento de Fisicoquímica, Facultad de Ciencias Químicas, Universidad Nacional de Córdoba, Haya de la Torre esq. Medina Allende, Ciudad Universitaria, X5000HUA Córdoba, Argentina
[b] INQUINOA (CONICET- UNT). Instituto de Química Física, Facultad de Bioquímica, Química y Farmacia, Universidad Nacional de Tucumán, San Lorenzo 456, T4000CAN Tucumán, Argentina
[c] Institut Néel, CNRS et Université Joseph Fourier, BP 166, 38042 Grenoble Cedex 9, France
[d] Departamento de Física. UEM. Av. Colombo, 5790, Maringá, PR, Brazil
[e] Instituto de Química Inorgánica; Facultad de Bioquímica, Química y Farmacia; Universidad Nacional de Tucumán. Ayacucho 471. 4000. San Miguel de Tucumán. Argentina
[f] Centro Atómico Bariloche, Comisión Nacional de Energía Atómica, CONICET and Instituto Balseiro, Universidad Nacional de Cuyo, (8400) San Carlos de Bariloche (RN), Argentina

ARTICLE INFO

Article history:
Received 26 November 2016
Received in revised form 16 June 2017
Accepted 29 June 2017
Available online 1 July 2017

Keywords:
Perovskites
Weak ferromangetism
Superparamagnetic clusters
Cobatites
Orthoferrites

ABSTRACT

$YFe_{1-x}Co_xO_3$ (x = 0, 0.3, 0.5, 0.7 and 1) perovskite solid solutions were synthesized by thermal decomposition of the cyano-metal complexes $Y[Fe_{1-x}Co_x(CN)_6]\cdot 4H_2O$. All perovskites belong to the orthorhombic *Pnma* space group. Mössbauer spectra at room temperature show that samples with low Co^{3+} content are magnetically ordered, while samples with high Co^{3+} content are paramagnetic. A clear decrease of the magnetic order temperature was observed by magnetization vs. temperature experiments. At high temperatures, $YFe_{0.3}Co_{0.7}O_3$ is paramagnetic and a non common increase of magnetization is observed. The later can be related to the thermal excitation of Co^{3+} in low spin (LS) configuration to intermediate (IS) or high spin (HS) configuration. Along the different compositions of $YFe_{1-x}Co_xO_3$ solid solutions there is a competition between weak ferromagnetism (WFM) and superparamagnetic (SPM) clusters. WFM due to Fe^{3+} cations prevail in rich Fe^{3+} samples (x = 0 and 0.3) and the Fe^{3+} cations that form SMP clusters prevail in the sample with x = 0.7. Besides, in the sample with x = 0.5 we postulate a slight prevalence of WFM due to Fe^{3+} cations. For $YFe_{1-x}Co_xO_3$ with x = 0.3, 0.5 and 0.7 neutron powder data at 2, 150 and 350 K were refined with the irreducible representation Γ_4 (A_x F_y G_z).

1. Introduction

Interest in rare-earths cobaltites $RCoO_3$ (R = rare earth cations and Y^{3+}) with perovskite type structure has been mainly associated with electric and magnetic transitions which are related to the ability of Co^{3+} to present various spin states, i.e. low-spin (LS), high-spin (HS) and intermediate-spin (IS). This happens because the crystal-field splitting Δ_{CF} between the t_{2g} and e_g states is only slightly larger than the Hund coupling energy and the system can be thermally excited to either HS or IS configuration. In $RCoO_3$, the ground state of the localized Co^{3+} ions is the nonmagnetic state (S = 0) that corresponds to the LS ($t_{2g}^6 e_g^0$) configuration. As mentioned above, the transition to a paramagnetic state is associated with a thermal excitation to the IS ($t_{2g}^5 e_g^1$, S = 1) or HS ($t_{2g}^4 e_g^2$, S = 2) Co^{3+} states [1].

The $LaCoO_3$ oxide presents a rhombohedral crystallographic structure with *R*-3*c* space group [1], and it is the most studied member of the family $RCoO_3$. In the other members with magnetic R^{3+} cations, their peculiar magnetic and electrical properties can be masked by the magnetic moments of the R^{3+}. $LaCoO_3$ is a Mott non-magnetic insulator at low temperature, since the ground state for the Co^{3+} ions (d^6) corresponds to the LS configuration. However, at low temperature, a weak ferromagnetism may be present because there are enough localized spins present at the surface [2].

* Corresponding authors.
E-mail addresses: rodo@cab.cnea.gov.ar (R.D. Sánchez), carbonio@fcq.unc.edu.ar (R.E. Carbonio).
[1] Members of the Research Career of CONICET.

http://dx.doi.org/10.1016/j.materresbull.2017.06.045
0025-5408/

Increasing the temperature, first, a transition to a paramagnetic state appears at around $T_1 \sim 100$ K, next a change in spin state is evidenced by a plateau in the susceptibility at around $T_2 \sim 500$ K where an insulator to metal (*I-M*) transition takes place. The spin state above 500 K is now commonly recognized as a HS state with S = 2 and supported by various experimental studies such as resistivity [3], photoemission [4], thermal expansion [5], and specific heat capacity [6] measurements. However, the first spin state change at around 100 K remains an open issue and has been the subject of intense debate.

Substitution of La^{3+} for rare earth or Y^{3+}cations with smaller ionic radii increases the cooperative rotations of the CoO_6 octahedra, reducing the Co—O—Co bond angles and the Co(*3d*)-O(*2p*)-Co(*3d*) interactions. This causes that the members of the family with rare earth ionic radii smaller than La^{3+} exhibit an orthorhombic crystallographic structure with *Pnma* space group and significant changes in the magnetic and electrical properties [7]. $RCoO_3$ (R = rare earth and Y^{3+}) also shows a spin state transition like $LaCoO_3$. The magnetic and *I-M* transitions shift systematically to higher temperatures with decreasing R^{3+} ionic radii. This indicates that the LS state of Co^{3+} ions in $RCoO_3$ perovskites with smaller rare earth ions becomes more stable compared to $LaCoO_3$ [7–12]. The physical reason for this behavior is the decrease of Co—O bond length due to the chemical pressure occurring with substitution of La^{3+} by smaller rare earth ions and hence the increase of the Δ_{CF} value and as a consequence stabilizing the LS state [13]. In particular, the magnetic susceptibility and lattice expansion data for $YCoO_3$ suggest that the diamagnetic-paramagnetic transition spreads over 450–900 K range. The *I-M* transition is centered at 750 K (inflection point of electrical resistivity) and occurs nearly simultaneously with the magnetic transition [14].

Changes in the Co—O bond length can also be induced by chemical substitution in the perovskite B position. In particular it was found that for $LaCo_{0.5}Ni_{0.5}O_3$ the population of Co e_g orbitals is larger than that of $LaCoO_3$ and this is evidenced by the fact that the unit cell volumes of $LaCoO_3$ and $LaNiO_3$ are smaller than those of $LaCo_{0.5}Ni_{0.5}O_3$ [15].

Furthermore, orthoferrites, $RFeO_3$ have been studied for a long time. This system is antiferromagnetic (AFM) due to the Fe^{3+}-O-Fe^{3+} superexchange interaction with a small canting of the Fe^{3+} magnetic moments due to an atisymmetric Dzyaloshinskii-Moriya interaction [16]. Until very recently, there has been no report of ferroelectricity in orthoferrites. This is because theoretically, ferroelectricity would be forbidden by their centrosymmetric *Pnma* structure. However in recent years, it was shown that some members of the $RFeO_3$ family (R = rare earth and Y) exhibit simultaneously weak ferromagnetism (WFM) and ferroelectricity at room temperature (R = Sm and Y) [17,18]. It was also reported the occurrence of ferroelectric polarization at the magnetic ordering temperature of the transition metal ions in the weak ferromagnetic $YCr_{1-x}M_xO_3$ (M = Fe or Mn) perovskite [19].

In the present article we have performed a detailed study of the crystal and magnetic structure of $YFe_{1-x}Co_xO_3$ (x = 0, 0.3, 0.5, 0.7 and 1) from powder neutron diffraction data complemented with magnetic measurements and Mössbauer spectroscopy (MS). Changes in magnetic properties and results of Mössbauer spectroscopy are discussed in terms of the random replacement of the magnetic Fe^{3+} ion by the non-magnetic Co^{3+} (LS) ion.

2. Experimental procedure

The cyano-metal complexes, $Y[Fe_{1-x}Co_x(CN)_6]\cdot 4H_2O$ ($0 \leq x \leq 1$), as precursors of perovskite-type oxides, $YFe_{1-x}Co_xO_3$, were prepared according to the reported method [20,21] slowly dropping a solution of $Y(NO_3)_3$ on a solution containing stoichiometric amounts of $K_3[Fe(CN)_6]$ and $K_3[Co(CN)_6]$ under continuous stirring at 60 °C for 2 h. The resulting precipitates were separated by filtration, washed with water and ethanol and finally stored in the dark in a dry box with silica gel. The precursor powders were heat-treated in a furnace at 950 °C during 6 h to yield perovskite-type oxides $YFe_{1-x}Co_xO_3$.

Room temperature MS measurements were performed in the transmission geometry, using a conventional spectrometer, operated in the constant acceleration mode. γ rays were provided by a ^{57}Co (Rh) source with an initial activity of 50 mCi. The velocity scale was calibrated by using a standard iron foil absorber. The Mössbauer spectra were analyzed with a non linear least square routine with Lorentzian line shapes. Hyperfine magnetic field distributions were occasionally traced by means of histograms with a fixed linewidth (Γ). All isomer shift (IS) data given in this paper are relative to α-Fe.

The Powder X-Ray Diffraction (PXRD) patterns were recorded at room temperature (RT) on a PANanalitycal X'Pert PRO diffractometer (in Bragg–Brentano geometry with Cu Kα radiation). For the structure refinements, the PXRD data were collected in the angular range 5–120° in steps of 0.02° and with a collection time of 10 s/

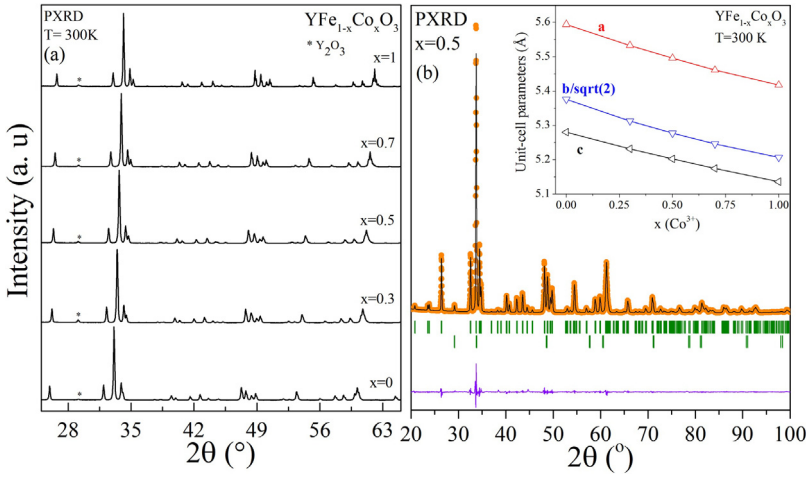

Fig. 1. (a) PXRD data for $YFe_{1-x}Co_xO_3$ (x = 0, 0.3, 0.5, 0.7 and 1). The star indicates the most intense reflection of Y_2O_3 (minor impurity). (b) Refined PXRD pattern of $YFe_{0.5}Co_{0.5}O_3$ sample at 300 K. Observed (cross), calculated (full line) and difference (bottom line). The first series of tick marks correspond to the Bragg reflections of the main $YFe_{0.5}Co_{0.5}O_3$ phase and the second series of Bragg positions correspond to the minor impurity Y_2O_3 (~1%). (*Inset*) Co^{3+} content dependence of the unit-cell parameters for $YFe_{1-x}Co_xO_3$ (x = 0, 0.3, 0.5, 0.7 and 1) samples.

step. Powder Neutron diffraction (PND) experiments were carried out on the powder diffractometer D1 B (λ=2.520 Å), the high-resolution powder diffractometer D2 B (λ=1.594 Å) and the high-flux diffractometer D20 (λ = 2.410 Å) at the Institute Laue-Langevin (ILL) in Grenoble (France). To study the thermal evolution of the crystallographic and magnetic structure its PND patterns were collected for $YFe_{1-x}Co_xO_3$ (x = 0.3, 0.5 and 0.7) at 2, 150 and 513 K in the D1 B instrument and at 350 K in the D2 B one. The 2θ range was 8.0 to 160°, with increments of 0.05°. The data collection time was approximately 2 h. A wavelength of 1.594 Å (in D2B) was used to determine the crystal structure whereas a large wavelength of 2.520 Å (in D1B) was chosen to study the magnetic structure.

The refinements of crystal structures from PXRD and PND data were performed by the Rietveld method [22] using the FULLPROF program [23]. A Thompson-Cox-Hastings pseudo-Voigt function was chosen to generate the line shape of the diffraction peaks. The following parameters were refined: scale factor, background coefficients, zero-shift, peak shape parameters, atomic positional and thermal factors, unit-cell parameters and occupancies of the rare-earth and transition metal cations.

Magnetic measurements were performed in a commercial Quantum Design MPMS-5S superconducting quantum interference device magnetometer (SQUID), on powdered samples, in the 5–350 K temperature range and magnetic fields up to 50 kOe. Isothermal magnetization curves were obtained for magnetic fields going from −50 kOe to 50 kOe at T = 5 K. The magnetic measurements in the 300–930 K temperature range were performed in a home-made Faraday balance under an applied magnetic field of 5 kOe.

3. Results and discussions

3.1. Structural refinements

The PXRD patterns for $YFe_{1-x}Co_xO_3$ are shown in Fig. 1(a). The patterns are similar to those of $YFeO_3$ and $YCoO_3$ previously assigned to an orthorhombic structure with space group *Pnma* [24–26]. In all the patterns, a minor impurity of Y_2O_3 was observed. The refinements of the crystal structure of the $YFe_{1-x}Co_xO_3$ oxides (x = 0, 0.3, 0.5, 0.7 and 1) were preliminary carried out from PXRD data. The structures were refined with orthorhombic symmetry and *Pnma* (#62) space group. Fe^{3+} and Co^{3+} cations were randomly placed at *4b (0, 0, 1/2)* sites, Y^{3+} and $O^{2-}(1)$ at *4c (x, 1/4, z)* sites and $O^{2-}(2)$ at *8d (x, y, z)* sites. Fig. 1(b) illustrates the good agreement between the observed and calculated PXRD patterns at RT for $YFe_{0.5}Co_{0.5}O_3$ (for the other samples a similar agreement was obtained). The refinements show ~1% of Y_2O_3 in all samples (see the second series of tick marks in Fig. 1(b)). The inset of Fig. 1(b) shows the Co^{3+} content dependence of unit-cell parameters for $YFe_{1-x}Co_xO_3$ samples. It is important to emphasize that the substitution of Fe^{3+} ion ($<r^{Fe3+}_{(HS)}> = 0.645$ Å) [27] by the smaller Co^{3+} ion ($<r^{Co3+}_{(LS)}> = 0.545$ Å, $<r^{Co3+}_{(IS)}> = 0.56$ Å and $<r^{Co3+}_{(HS)}> = 0.61$ Å) [28] leads to decrease of unit cell parameters following the Vegard's law for ideal solid solutions.

In order to obtain a complete crystal structure refinement and the refined chemical formula for the intermediate samples (x = 0.3, 0.5 and 0.7) the PND patterns were refined. Fig. 2 shows the refined PND pattern at 350 K for $YFe_{0.7}Co_{0.3}O_3$ compound. We must emphasize that the refinement of the Fe/Co occupancy in the same crystallographic site is impossible by using PXRD data because X-ray scattering factors for Fe^{3+} and Co^{3+} ions are very similar. However, these occupancies can be determined, in a very precise way, by PND due to the high difference in the scattering lengths for Fe and Co (0.945 fm and 0.249 fm, respectively). Table 1 summarizes the unit-cell parameters, atomic positions, occupancies, displacement parameters and discrepancy factors obtained by the Rietveld refinement of PND data of $YFe_{1-x}Co_xO_3$ (x = 0.3, 0.5 and 0.7) at 350 and 2 K. Besides, Table 1 shows the refined chemical formula obtained for each sample. The formulas obtained were in excellent agreement with the nominal compositions.

3.2. Mössbauer spectroscopy

The RT Mössbauer spectra of the $YFe_{1-x}Co_xO_3$ (x = 0, 0.3, 0.5 and 0.7) solid solutions are shown in Fig. 3. The spectrum of $YFeO_3$ shows a single magnetic sextet characteristic of Fe^{3+} ions. The isomer shift (IS), quadrupolar splitting (QS), line width (Γ) and area are given in Table 2. The small line width (Γ = 0.32 mm/s) of the spectrum shows that the sample exhibits excellent crystallinity, in agreement with PXRD data discussed above. The hyperfine field value is similar to the value reported by Mathur *et. al* [24], which might be attributed to a high local atomic order in the sample that favours the Fe^{3+}-O^{2-}-Fe^{+3} superexchange interactions.

The spectrum of $YFe_{0.7}Co_{0.3}O_3$ shows a hyperfine magnetic structure with broadened and slightly asymmetric lines and was fitted with a hyperfine magnetic field distribution.

The spectra of $YFe_{0.5}Co_{0.5}O_3$ and $YFe_{0.3}Co_{0.7}O_3$ show quadrupole doublets corresponding to paramagnetic Fe^{3+} in high-spin state. A

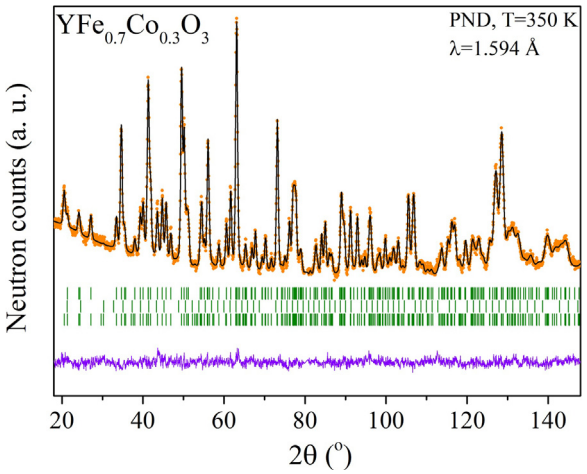

Fig. 2. Refined PND pattern of $YFe_{0.7}Co_{0.3}O_3$ sample at 350 K. Observed (circles), calculated (full line) and difference (bottom line). The first series of tick marks correspond to the Bragg reflections of the main $YFe_{0.7}Co_{0.3}O_3$ phase, the second series of Bragg positions correspond to the minor impurity Y_2O_3 and the third series of Bragg positions correspond to the magnetic structure reflections of the main $YFe_{0.7}Co_{0.3}O_3$ phase.

Table 1
Unit-cell parameters, atomic positions, occupancies, displacement parameters, discrepancy factors and the refined chemical formula obtained by the Rietveld refinement from PND data of YFe1-xCoxO3 (x = 0.3, 0.5 and 0.7) at 350 and 2 K.

x	0.3		0.5		0.7	
T (K)	350	2	350	2	350	2
a (Å)	5.5360 (2)	5.5343 (2)	5.4922 (2)	5.4909 (3)	5.4622 (3)	5.4548 (2)
b (Å)	7.5210 (3)	7.5055 (3)	7.4620 (4)	7.4467 (4)	7.4216 (4)	7.4001 (4)
c (Å)	5.2363 (2)	5.2249 (2)	5.2023 (2)	5.1893 (2)	5.1792 (2)	5.1621 (2)
V (Å^3)	218.02 (4)	217.03 (2)	213.21 (2)	212.19 (2)	209.96 (2)	208.37 (2)
Y^{3+} 4c (x, 1/4, z)						
x	0.0679 (3)	0.0684 (4)	0.0669 (3)	0.0681 (3)	0.0666 (4)	0.0681 (3)
z	0.9839 (6)	0.9809 (7)	0.9831 (5)	0.9832 (6)	0.9818 (6)	0.9827 (6)
B (Å^2)	0.51 (7)	0.48 (9)	0.60 (9)	0.44 (9)	0.51 (1)	0.20 (2)
(Fe, Co) 4b (0, 0, 1/2)						
B (Å^2)	0.67 (6)	0.75 (7)	0.90 (8)	0.80 (9)	0.90(1)	0.70 (1)
Occup. (%)	0.694(2)/0.306(2)	0.694(2)/0.306(2)	0.490(2)/0.510(2)	0.490(2)/0.510(2)	0.290(2)/0.710(2)	0.290(2)/0.710(2)
O1 4c (x, 1/4, z)						
x	0.4643 (5)	0.4630 (6)	0.4675 (5)	0.4658 (5)	0.4689 (6)	0.4687 (5)
z	0.1007 (5)	0.1018 (7)	0.0974 (5)	0.0980 (6)	0.0939 (7)	0.0961 (6)
B (Å^2)	0.56 (9)	0.49 (2)	0.99 (9)	0.84 (9)	0.80 (1)	0.50 (1)
O2 8d (x, y, z)						
x	0.6969 (4)	0.6981 (4)	0.6984 (3)	0.6974 (4)	0.6981 (4)	0.6979 (4)
y	0.9464 (3)	0.9456 (3)	0.9477 (2)	0.94766 (3)	0.9491 (3)	0.9490 (3)
z	0.3073 (4)	0.3075 (4)	0.3066 (3)	0.3072 (4)	0.3068 (5)	0.3075 (4)
B (Å^2)	0.41 (9)	0.10 (2)	0.49 (9)	0.36 (1)	0.91 (1)	0.51 (2)
Reliability factors						
χ^2	3.71	11.7	9.90	9.86	5.29	3.39
R_p (%)	6.97	6.24	6.17	5.90	9	8.59
R_{wp} (%)	7.77	8.55	7.75	8.20	10.6	7.67
R_{exp} (%)	4.03	2.50	2.46	2.16	4.62	4.16
R_{Bragg} (%)	2.10	2.71	2.71	2.31	2.10	2.92
Ref. Chem. Form.	$YFe_{0.69(2)}Co_{0.31(2)}O_3$		$YFe_{0.49(2)}Co_{0.51(2)}O_3$		$YFe_{0.29(2)}Co_{0.71(2)}O_3$	

magnetic component is slightly visible in $YFe_{0.5}Co_{0.5}O_3$ (not high enough to obtain refined parameters) although disappeared in $YFe_{0.3}Co_{0.7}O_3$, indicating that Fe^{3+} is mainly in the paramagnetic state. This can be explained because the Fe diluted compound $YFe_{0.3}Co_{0.7}O_3$ has Fe^{3+} mainly surrounded by Co^{3+} ions.

3.3. Magnetic characterization

The thermal evolution of ZFC and FC DC magnetic susceptibility were measured for all members of the $YFe_{1-x}Co_xO_3$ family in the temperature range 5–350 K (H = 500 Oe and 50 kOe) and 300–930 K (H = 5 kOe). Fig. 4 illustrates the ZFC-FC curves at temperatures higher than RT.

The curves for $YFeO_3$ (x = 0) show an abrupt increase of magnetization at temperatures lower than $T_N \sim 675$ K suggesting the onset of magnetic ordering. The ZFC-FC curves overlap at temperatures higher than T_N and diverge when the temperature decreases below this value. When Fe^{3+} cation is replaced by Co^{3+} cation the onset of magnetic order (T_N) appears at lower temperatures and the magnitude of the increase of magnetization is smaller, suggesting that an AFM order predominates in the samples. The ZFC-FC curves for $YFe_{0.7}Co_{0.3}O_3$ (x = 0.3) overlap at temperatures higher than $T_N \sim 480$ K and the magnetization shows a clear increment at temperatures lower than T_N. In both samples (x = 0 and 0.3) the increment of the magnetization below T_N denotes the occurrence of a ferrimagnetic component that comes from the canting of the transition metals magnetic moments with AFM order (WFM) due to the Dzialoshinsky–Moriya antisymmetric exchange interactions [16]. Furthermore, the important divergence between the ZFC and FC curves below T_N evidence some kind of magnetic frustration on the ferromagnetic component.

For the samples with x = 0.5 and 0.7, it is presumed that the magnetic order temperatures are below RT. Fig. 5(a) shows the ZFC-FC curves collected at 500 Oe in the temperature range from 4 to 350 K for $YFe_{0.5}Co_{0.5}O_3$ and $YCoO_3$. The ZFC-FC curves for $YFe_{0.5}Co_{0.5}O_3$ exhibit an increment of magnetization at $T_N \sim 240$ K. As can be observed in Fig. 5(a), the onset of shift between the ZFC and FC curves happen at $T > T_N$. It is postulated that the reason for this shift at $T > T_N$ is related with the presence of a small amount of an impurity phase with garnet structure $Y_3Fe_5O_{12}$ (magnetic order temperature ~500 K) [29], not detected in the PXRD and PND patterns (the dashed line shows the corrected FC curve taking into account the magnetization of this impurity). The inset of Fig. 5(a) shows the inverse of the magnetic susceptibility (calculated from the ZFC and FC curves measured at 50 kOe) as a function of temperature for $YFe_{0.5}Co_{0.5}O_3$. A clear change in the curve slope at $T_N \sim 240$ K is observed, in perfect agreement with the curve collected at 500 Oe. Moreover, this magnetic order temperature is in perfect agreement with the one recently published by other authors for $YFe_{0.5}Co_{0.5}O_3$ [30].

Fig. 5(b) shows the ZFC-FC curves collected at 500 Oe in the temperature range from 4 to 350 K for $YFe_{0.3}Co_{0.7}O_3$ and $YCoO_3$ samples. For $YCoO_3$ a very small magnetization at low temperatures is observed, suggesting the possibility of Co^{3+} in LS configuration (S = 0). In $YFe_{0.3}Co_{0.7}O_3$ a clear paramagnetic behavior is observed. However, in the magnetization curves of both samples a slight separation between the ZFC and FC curves is observed (see detail for $YCoO_3$ in the upper inset of Fig. 5(b)). This separation was informed previously for $YCoO_3$ [26], and the authors suggested that could be attributed to the weak ferromagnetism generated at the surface, as it was informed in the analogous $LaCoO_3$ [2]. The slight separation between the ZFC and

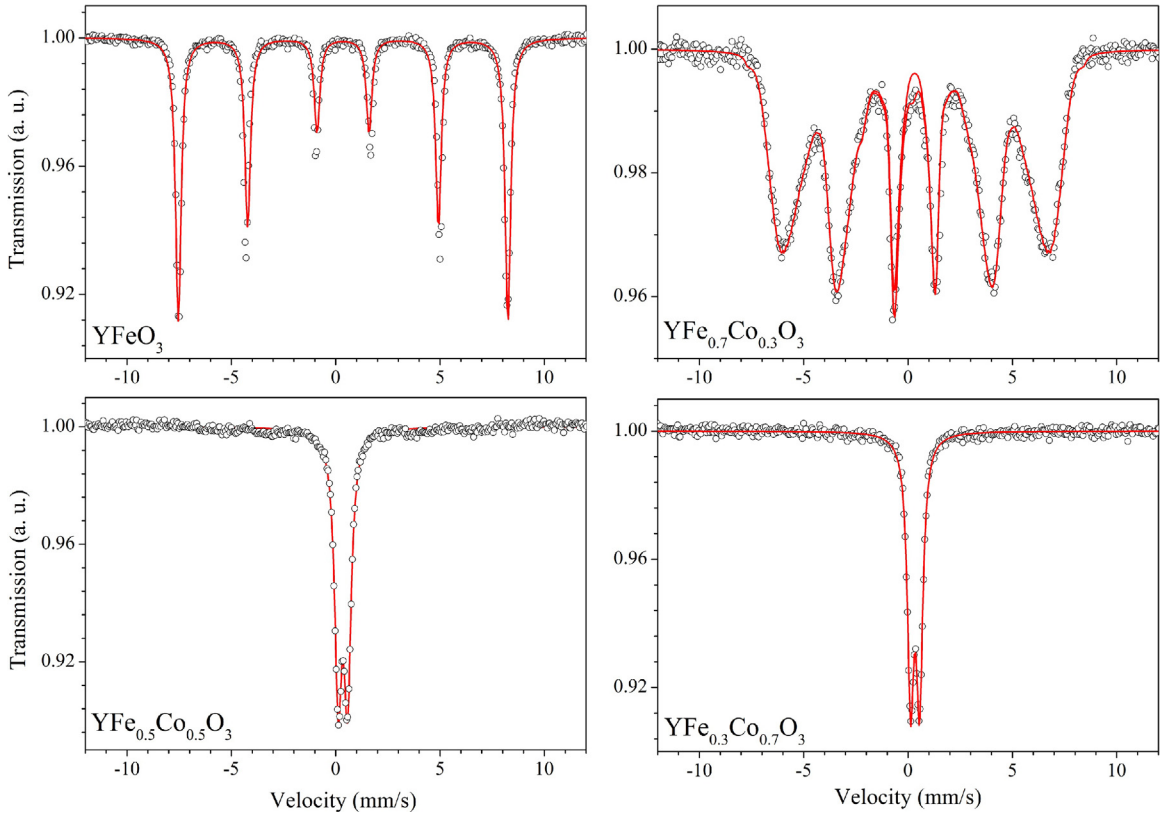

Fig. 3. RT ^{57}Fe Mössbauer spectra of the solid solutions $YFe_{1-x}Co_xO_3$ (x = 0, 0.3, 0.5 and 0.7).

Table 2
Mössbauer parameters of the $YFe_{1-x}Co_xO_3$ solid solutions at room temperature. IS: isomer shift, QS: quadrupolar shift and Γ: line width.

Compound	Fe site	IS (mm/s)	QS(mm/s)	Γ(mm/s)	Area (%)
$YFeO_3$	Fe(1)	0.35	0.00	0.32	100
$YFe_{0.7}Co_{0.3}O_3$	Fe(1)	0.34	0.05	0.28	100
$YFe_{0.5}Co_{0.5}O_3$	Fe(1)	0.34	0.45	0.41	100
$YFe_{0.3}Co_{0.7}O_3$	Fe(1)	0.34	−0.43	0.38	100

FC curves observed in $YFe_{0.3}Co_{0.7}O_3$ could have a similar origin to that in $YCoO_3$, but in this sample the presence of a trace amount of the magnetic impurity $Y_3Fe_5O_{12}$ is not ruled out [29]. The paramagnetic (PM) behavior observed in $YFe_{0.3}Co_{0.7}O_3$ suggests that below RT the Co^{3+} ions are in the non-magnetic LS state. Besides, the Fe^{3+} concentration (1-x = 0.3) in this sample is very close to the percolation threshold limit (1-x ~ 0.33) for a 3D system as the perovskite structure. This describes the point at which the Fe^{3+}-O-Fe^{3+} super-exchange paths can be magnetically ordered along the crystal without interruptions due to the dopant ion (Co^{3+}) [31,32]. However, the inverse of the magnetic susceptibility as a function of temperature for $YFe_{0.3}Co_{0.7}O_3$ only has a linear behavior typical for paramagnets at T > 170 K (lower inset of Fig. 5(b)), and below 170 K a small change in the slope of the curve is observed. This change in the slope may indicate the onset of magnetic order.

As stated above, for $YCoO_3$ a very small magnetization is observed at low temperatures, suggesting the possibility of Co^{3+} in LS state (S = 0) contribution in the surface of the grains. Nevertheless, as can be observed in the upper inset of Fig. 4, at high temperatures (higher than ~600 K) an increase of magnetization is observed which can be related to the thermal excitation of Co^{3+} in LS configuration to IS or HS. The same behavior was observed by Knížek et al. [26]. As can be observed in the upper inset of Fig. 4, in $YFe_{0.3}Co_{0.7}O_3$ an increase of magnetization at very high temperatures (around 850 K) is also observed. The lower inset of Fig. 4 shows that there is not a linear behavior of the inverse susceptibility curve that follows the Curie-Weiss law ($\chi C/(T-\theta)$) (where C is the Curie constant and θ is the Weiss temperature) in these two samples (x = 1 and 0.7). On the other hand, for the samples with x = 0.3 and 0 (samples rich in Fe^{3+} ion) there is a linear behavior of the inverse susceptibility curve that follows the Curie-Weiss law. The effective paramagnetic moment and Weiss temperature determined from the fits are 6.05 μ_B and −1287 K for $YFeO_3$ and 5.52 μ_B and −1796 K for $YFe_{0.7}Co_{0.3}O_3$. The magnetic response should be due only to the paramagnetic moments of the Fe^{3+} (HS configuration) if the Co^{3+} cations are in the LS state. On the other hand Co^{3+} cations can contribute to the magnetic response if they are in the IS (S = 1) or the HS (S = 2) state. The expected effective paramagnetic moment for $YFeO_3$ is 5.92 μ_B. This value is in good agreement with the experimental paramagnetic moment obtained from the Curie-Weiss fit (6.05 μ_B). The expected effective paramagnetic moment for $YFe_{0.7}Co_{0.3}O_3$ can be estimated as $\mu_{eff} = [0.7\ \mu_{eff}^2(Fe^{3+}) + 0.3\ \mu_{eff}^2(Co^{3+})]^{1/2}$. The obtained values for Co^{3+} ion in IS and HS are 2.83 μ_B and 4.89 μ_B, respectively. The experimental effective paramagnetic moment for $YFe_{0.7}Co_{0.3}O_3$ (5.52 μB) is in better agreement with the expected one calculated for Co^{3+} (HS) (5.63 μ_B) (the expected one calculated for Co^{3+} (IS) was 5.19 μ_B). This result is not surprising, since the Curie-Weiss Law is fitted at high temperatures, where the HS state of Co^{3+} is highly populated.

The isothermal magnetization curves measured at 5 K are displayed in Fig. 6(a) and 6(b). All the samples show an antiferromagnetic canted (or weak ferromagnetic) behavior. As stated above, the canted antiferromagnetism observed in our compounds is similar to that proposed in orthoferrites due to the DM antisymmetric exchange interactions [16]. In the samples with

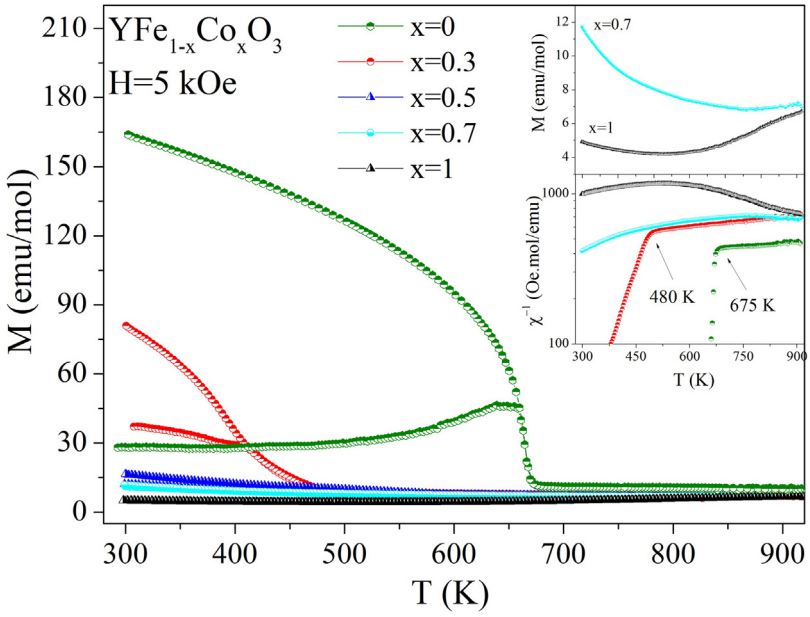

Fig. 4. ZFC-FC curves at temperatures higher than room temperature and H = 5 kOe for $YFe_{1-x}Co_xO_3$ (x = 0, 0.3, 0.5, 0.7 and 1) samples. (*Upper inset*) Zoom view of the FC curves for the samples with x = 0.7 and 1. (*Lower inset*) Temperature dependences of the inverse of the magnetic susceptibility for $YFe_{1-x}Co_xO_3$ (x = 0, 0.3, 0.7 and 1) samples.

x = 0, 0.3 and 0.5 the magnetization curves exhibit an obvious hysteresis loop, but for the sample with x = 0.7 there is no hysteresis (see Fig. 6(b)). In all samples perfect saturation is not reached up to H = 50 kOe, instead the magnetization increases linearly in the region of higher magnetic field. This kind of magnetization loops and the linear dependence at high fields are usually attributed to the weak ferromagnetism caused by a departure from the collinearity of the magnetic moments in an antiferromagnet [33]. Therefore, the high field part of M (H) curves can be represented as $M = \chi_{AFM}H + \sigma_S$, where $\chi_{AFM}H$ is the AFM contribution and σ_S is the saturation magnetization of the weak ferromagnetism [34]. Thus, the ferromagnetic component can be obtained by subtracting the AFM contribution from the total magnetization.

At 5 K, the Co^{3+} ions are present in the non magnetic LS state and the magnetic response is solely due to the Fe^{3+}-O^{2-}-Fe^{3+} super-exchange interactions. In the canted G-type AFM structure of $YFeO_3$ (x = 0), each Fe^{3+} ion is surrounded by six O^{2-} ions arranged in FeO_6 octahedra, and the O^{2-} is the common apex of the two adjacent octahedra, functioning as a superexchange interaction bond. Due to the DM antisymmetric exchange mechanism, each Fe^{3+} magnetic moment is arranged not totally antiparallel, but normally canted at a small angle. As mentioned above, this arrangement of Fe^{3+} magnetic moment leads to the occurrence of WFM. When Fe^{3+} are continuously replaced in a random way by Co^{3+} (in the LS state at 5 K) a distribution of Fe^{3+} and Co^{3+} is formed and there are some rich regions of Fe^{3+} cations (Fe^{3+}-O^{2-}-Fe^{3+} interactions), other rich regions in Fe^{3+}-O^{2-}-Co^{3+}-O^{2-}-Fe^{3+} interactions and additional rich regions of Co^{3+} (LS) cations, Co^{3+}-O^{2-}-Co^{3+}-O^{2-}- Co^{3+} interactions.

As can be seen in Fig. 7(b), H_c decreases when the content of Co^{3+} ion increases. It is clear that for the compounds with x = 0 and 0.3, each FeO_6 octahedra are entirely, or almost entirely, surrounded by other FeO_6 octahedra and the prevalent interactions are Fe^{3+}-O^{2-}-Fe^{3+} ones so Fe^{3+} magnetic moments are ordered AFM each other with a small FM component (WFM). The high H_c values presented by these compounds (x = 0 and 0.3) indicate a higher magnetic anisotropy than the other members of the family. When the Co^{3+} content increases in the samples, the weak ferromagnetic regions Fe^{3+}-O^{2-}-Fe^{3+} become smaller and the resultant magnetic domains are more easily reverted. At the same time, the regions where the Co^{3+} is dominant grow up. These last regions will leave regions with Fe^{3+}-O^{2-}-Fe^{3+} interactions (WFM) and Fe^{3+} totally isolated with PM behavior. As can be observed in Fig. 6(b), in the case of the compound with x = 0.5, the weak ferromagnetic regions still prevail and this is evident at low magnetic fields in the hysteresis loop. On the other hand, in the sample with x = 0.7 the hysteresis loop is not observed.

As can be seen in Fig. 7(a), for the samples with x = 0 and 0.3, σ_s decrease with *x*. In these samples σ_s comes from the weak ferromagnetic component. When the Co^{3+} content increases (x = 0.5 and 0.7), M at high field increases (Fig. 6). As we will see later, a portion of all the Fe^{3+} cations present in these samples generates ferromagnetic clusters in superparamagnetic (SPM) state.

To obtain information about the SPM clusters present in the analyzed samples, the M vs. H curves for the samples with x = 0.5 and 0.7 can be described with a Langevin's function with an extra linear component ($M = a[coth(bH/T)-(bH/T)^{-1}] + cH/T$). The two first terms are the Langevin's function that describes the super-paramagnetic behavior which is usually found in magnetic clusters or small particles systems [35]. The last term is a paramagnetic contribution due to isolated and non interacting Fe^{3+} ions. The parameter *a* is the maximum saturation magnetization (σ_s^{SPM}) reached by the clusters when these are aligned with a high magnetic field; *b* is a parameter associated with the total magnetic moment of each cluster ($b = \mu/k_B$) and *c* is the fraction of non-correlated or isolated Fe^{3+} cations.

In the case of $YFe_{0.5}Co_{0.5}O_3$ the saturation reached for the clusters is $\sigma_s^{SPM} = 0.0473\ \mu_B$/mol and we obtained from the fitting that 3% of the Fe^{3+} are in clusters with a total magnetic moment around 7 μ_B/cluster (close to 2 Fe^{3+}/cluster). Thus, the remaining 97% of Fe^{3+} in the sample has to be distributed between the WFM and PM. In the case of $YFe_{0.3}Co_{0.7}O_3$ the saturation reached for the clusters is $\sigma_s^{SPM} = 0.1310\ \mu_B$/mol and we obtained from the fitting that 9% of the Fe^{3+} are in clusters with a total magnetic moment around 153 μ_B/cluster (close to 31 Fe^{3+}/cluster). Thus, the remaining 91% of Fe^{3+} cations in the sample has to be distributed between the WFM and PM. As was proposed previously for

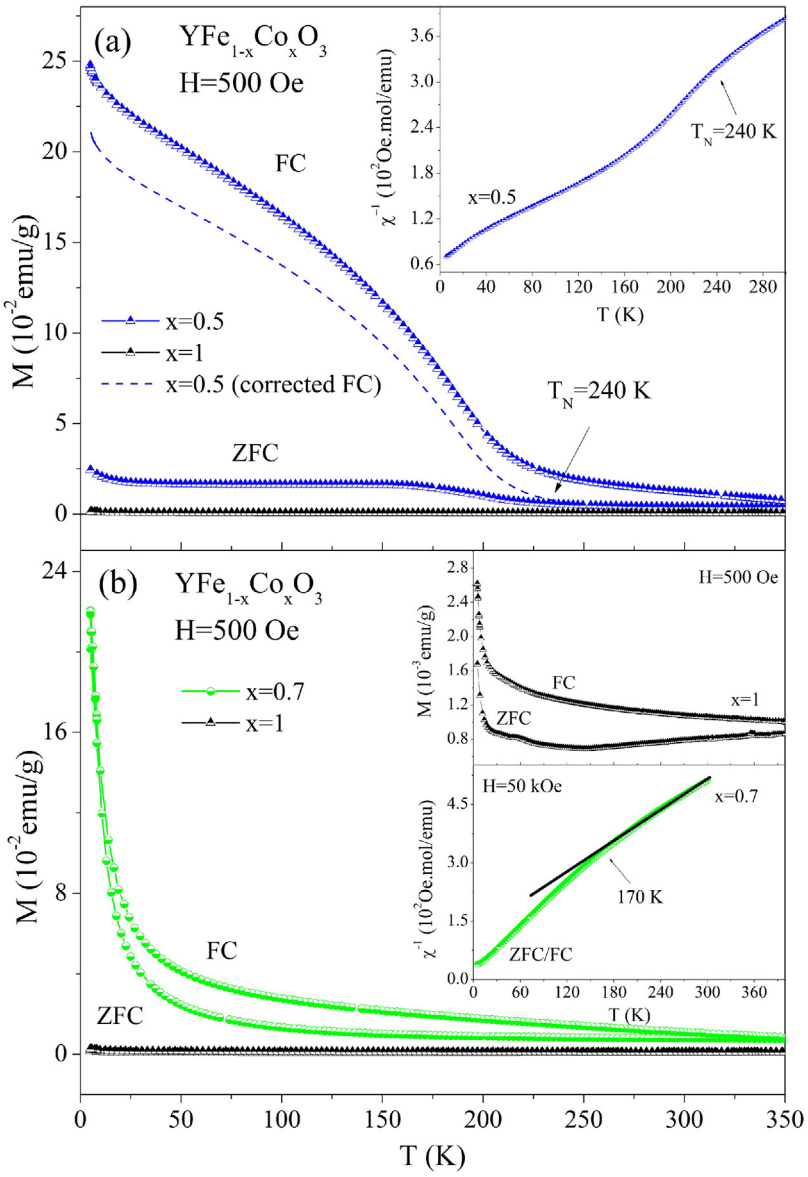

Fig. 5. (a) ZFC-FC curves at temperatures lower than room temperature and H = 500 Oe for $YFe_{0.5}Co_{0.5}O_3$ and $YCoO_3$ samples. The dashed line shows the corrected FC curve. (*Inset*) Inverse of the magnetic susceptibility, calculated from the ZFC and FC curves measured at 50 kOe, as a function of temperature for $YFe_{0.5}Co_{0.5}O_3$. (b) ZFC-FC curves at temperatures lower than room temperature and H = 500 Oe for $YFe_{0.3}Co_{0.7}O_3$ and $YCoO_3$ samples. (*Upper inset*) Zoom view of the ZFC-FC curves for $YCoO_3$. (*Lower inset*) Inverse of the magnetic susceptibility, calculated from the ZFC and FC curves measured at 50 kOe, as a function of temperature for $YFe_{0.3}Co_{0.7}O_3$.

different perovskites [36,37], an explanation for the SPM observed in the small clusters is that they have different amounts of spin up and spin down.

Fig. 7(a) shows the σ_s^{SPM} (obtained from the fit with a Langevin's function with an extra linear component) and σ_s^{WFM} (obtained with the rest of the Langevin's function with an extra linear component to the total magnetization) for the samples with x = 0.5 and 0.7. As can be seen, σ_s^{SPM} increases with the Co^{3+} content, whereas the σ_s^{WFM} decreases. This shows that along the $YFe_{1-x}Co_xO_3$ solid solution there is a competition between the WFM and the SPM clusters. The weak ferromagnetic Fe^{3+} cations prevail in the rich Fe^{3+} samples (x = 0 and 0.3) and the Fe^{3+} cations that form SMP clusters prevail in the sample with x = 0.7. Besides, in the sample with x = 0.5 we postulate a slight prevalence of the weak ferromagnetic Fe^{3+} cations.

Fig. 8 shows a magnetic phase diagram that summarizes the main magnetic characteristic of the $YFe_{1-x}Co_xO_3$ compounds. In this figure, the coexistence between the two magnetic phases (WFM and SPM clusters) for intermediate compositions is displayed.

3.4. Refinement of magnetic structure by powder neutron diffraction

The magnetic structure refinement of the $YFe_{1-x}Co_xO_3$ samples (x = 0.3, 0.5 and 0.7) was carried out from a set of PND patterns obtained at the D1 B diffractometer (λ=2.520 Å) in the range 2–513 K.

Fig. 9 shows the refined PND patterns at 2, 150, 350 and 513 K for $YFe_{0.5}Co_{0.5}O_3$, where new peaks of magnetic ordering appear at positions forbidden by the space group *Pnma* (i.e. the 110 refection) and the intensity of the 011 and 211 structural reflections increase when temperature decreases. In particular, the new peak corresponding to the 110 reflection appears in the pattern at 350 K and it grows when the temperature drops, together with the

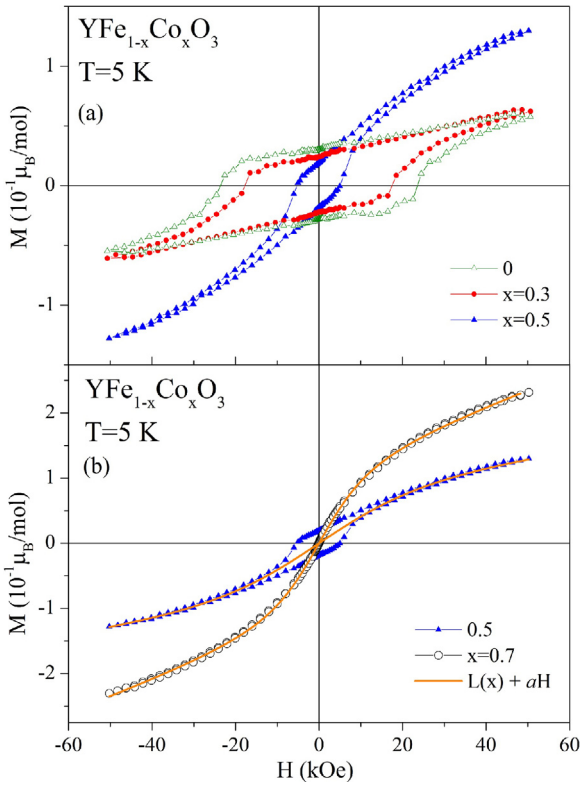

Fig. 6. (a) Magnetization vs. magnetic field isotherm at T = 5 K for $YFe_{1-x}Co_xO_3$ (x = 0, 0.3 and 0.5) samples. (b) Magnetization vs. magnetic field isotherm at T = 5 K for $YFe_{1-x}Co_xO_3$ (x = 0.5 and 0.7) samples. The orange line described the Langevin's function with an extra linear component. (For interpretation of the references to colour in this figure legend, the reader is referred to the web version of this article.)

increase of 011 and 211 reflections. For this sample the new peaks disappear in the pattern at 400 K, the same behavior is observed in the samples with x = 0.7, which results in a null refined magnetic moment. In the sample with x = 0.3 at 400 K these magnetic peaks are still visible. This implies the establishment of a long-range magnetic order at temperatures approaching 350 K in samples with x = 0.5 and 0.7 and temperatures larger than 400 K (and lower than 513 K) in the one with x = 0.3. It is important to note that the temperatures at which the magnetic peaks appear are somewhat higher than T_N (see Magnetic characterization section). The origin of these peaks can be understood based on the Fe^{3+}-O^{2-}-Fe^{3+} superexchange interactions and the random distribution of Fe^{3+} and Co^{3+} cations at the B-site of the perovskite structure as was observed by others authors in $YCr_{0.5}Fe_{0.5}O_3$ [19]. On the other hand,

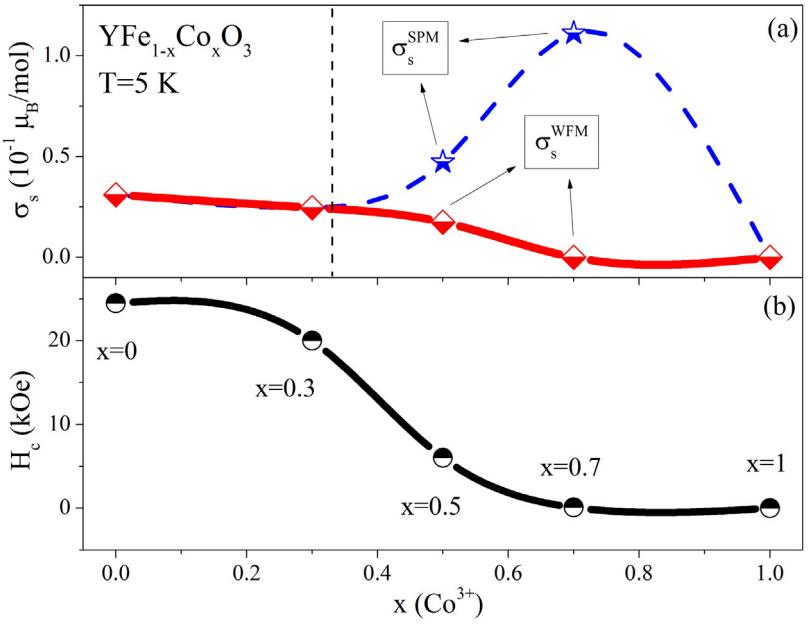

Fig. 7. (a) Co^{3+} content dependences of the saturation magnetization (σ_s). The vertical dashed line indicates the beginning of the SPM behavior. (b) Co^{3+} content dependence of the coercive magnetic field (H_c).

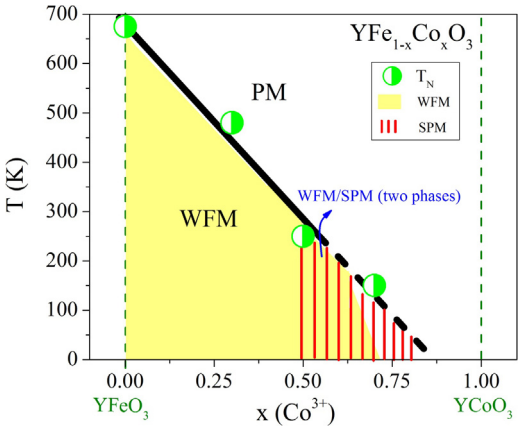

Fig. 8. Magnetic phase diagram for $YFe_{1-x}Co_xO_3$ samples.

these results are in good agreement with the ones obtained from Mössbauer spectroscopy at 300 K (see Fig. 3).

The different magnetic groups associated with the propagation vector $k = (0, 0, 0)$ for the magnetic transition which are compatible with the *Pnma* space group have been tabulated by Bertaut [38] and gives for the transition cations 4 irreducible representations allowing a non-zero magnetic contribution. The B-site magnetic cations are present at *4b* sites at positions S1 (0, 0, 1/2), S2 (1/2, 0, 0), S3 (0, 1/2, 1/2) and S4 (1/2, 1/2, 0), depending on the relative spin directions at the four positions. Four base vectors representing the possible magnetic modes of coupling can be expressed according to Bertaut's notation,

$$F = +S1 + S2 + S3 + S4,$$

$$G = +S1 - S2 - S3 + S4,$$

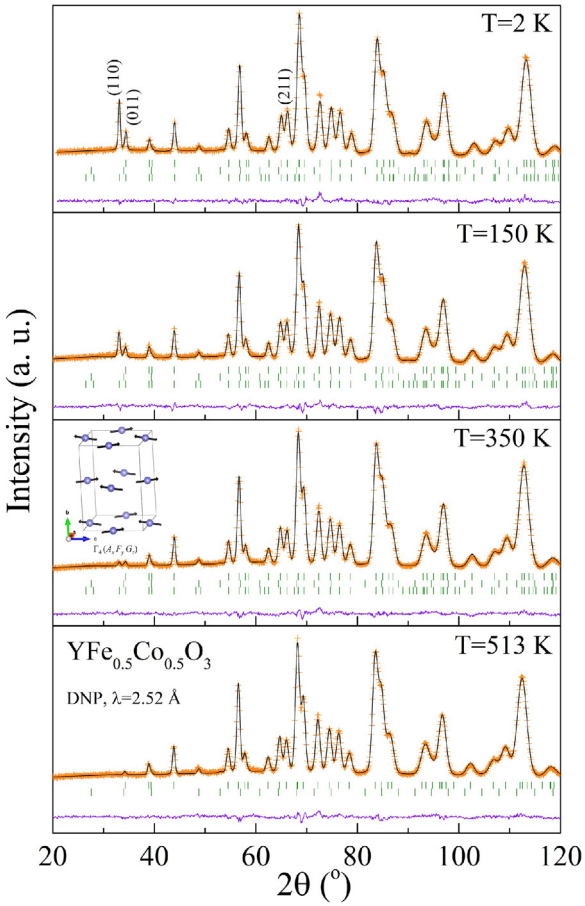

Fig. 9. Comparison of the PND refined patterns of $YFe_{0.5}Co_{0.5}O_3$ at 2 K, 150 K, 350 K and 513 K. Observed (circles), calculated (full line) and difference (bottom line). In each pattern the first series of tick marks correspond to the Bragg reflections of the main $YFe_{0.5}Co_{0.5}O_3$ phase and the second series of Bragg positions correspond to the minor impurity Y_2O_3. In the patterns at 2 K, 150 K and 350 K the third series of Bragg positions correspond to the Bragg reflections of the magnetic structure of the main $YFe_{0.5}Co_{0.5}O_3$ phase.

C = + S1 − S2 + S3 − S4,

A = + S1 + S2 − S3 − S4,

The four irreducible representations known for orthoferrites can be represented in terms of vector components F, G, C and A along three crystallographic directions. According to Bertaut's notations, these are defined as Γ_1 ($G_x C_y A_z$), Γ_2 ($C_x G_y F_z$), Γ_3 ($F_x A_y C_z$) and Γ_4 ($A_x F_y G_z$).

For the three $YFe_{1-x}Co_xO_3$ samples the neutron data at 2, 150 and 350 K were refined with the irreducible representation Γ_4 ($A_x F_y G_z$). In this structure, the magnetic moments are mainly oriented in an antiferromagnetic arrangement along the *z*-direction with a small canting along *y*-direction (the magnetic moment component along the *x*-direction is negligible). Fig. 9 shows an example of the good agreement between the observed and calculated PND patterns after refinement of the $YFe_{0.5}Co_{0.5}O_3$ magnetic structure at 2, 150 and 350 K. The pattern at 513 K was perfectly refined without a magnetic structure contribution.

In previous studies [39,40], it was found that in $YFe_{1-x}Mn_xO_3$ ($0 \leq x \leq 0.45$) and $RFe_{0.5}Cr_{0.5}O_3$ (R = Yb and Tm) a progressive spin-reorientation transition occurs and this was evident in the PND patterns with the reversion on the intensities of the (110) and (011) reflections when temperature decreases. In the case of $YFe_{1-x}Co_xO_3$ this was not observed, so spin-reorientation transition is absent and this is in agreement with the magnetization measurements that do not show spin-reorientation transition.

4. Conclusions

$YFe_{1-x}Co_xO_3$ (x = 0, 0.3, 0.5, 0.7 and 1) perovskite solid solutions were synthesized by thermal decomposition of the cyano-metal complexes $Y[Fe_{1-x}Co_x(CN)_6]\cdot 4H_2O$ at 950 °C for 6 h. All perovskites belong to the orthorhombic *Pnma* (#62) space group. The refined chemical formulas obtained in the compounds with x = 0.3, 0.5 and 0.7 were in an excellent agreement with the nominal compositions.

A well-developed magnetic order was observed in the RT Mössbauer spectra only in the samples with x = 0 and 0.3, while in the compounds with x = 0.5 and 0.7 quadrupole doublets corresponding to paramagnetic Fe^{3+} in high spin state was observed.

A clear decrease of the magnetic order temperature was observed when the Co^{3+} content increases. In $YCoO_3$ a very small magnetization was observed at low temperatures, suggesting the possibility of Co^{3+} in LS state (S = 0). In $YFe_{0.3}Co_{0.7}O_3$ a paramagnetic behavior was observed. This suggested that below RT Co^{3+} ions are in the non-magnetic LS state, because Fe^{3+} concentration (1-*x* = 0.3) in this sample is very close to the percolation threshold limit for perovskite structure. However, a small change in the slope of the inverse of the magnetic susceptibility as a function of temperature was observed at $T < 170$ K, which could indicate the onset of magnetic order. Besides, in $YCoO_3$ and $YFe_{0.3}Co_{0.7}O_3$ an increase of magnetization at high temperatures was observed and this can be associated to the thermal excitation of Co^{3+} in LS configuration to IS or HS configuration.

Along the $YFe_{1-x}Co_xO_3$ solid solution there is a competition between WFM and SPM clusters. WFM Fe^{3+} cations predominate in the rich Fe^{3+} samples (x = 0 and 0.3) and the Fe^{3+} cations that form SPM clusters predominate in the sample with x = 0.7. Besides, in the sample with x = 0.5 a coexistence between the two magnetic phases was suggested.

For the $YFe_{1-x}Co_xO_3$ samples with x = 0.3, 0.5 and 0.7 the neutron data at 2, 150 and 350 K were refined with the irreducible representation Γ_4 ($A_x F_y G_z$). In this structure, the moments are mainly oriented in an antiferromagnetic arrangement along the *z*-direction with a small canting along the *y*-direction.

Acknowledgements

F. P. and D. M. G. have contributed equally to this manuscript. R. E.C. thanks support from Consejo Nacional de Investigaciones Científicas y Técnicas (CONICET), PIP # 11220120100360, the Agencia Nacional de Promoción Científica y Tecnológica (ANPCyT), PICT-2013-2149 and the Secretaría de Ciencia y Tecnología de la Universidad Nacional de Córdoba (SECyT-UNC), Project 203/14. R. D.S. acknowledges support from ANPCyT, PICT 2011-752, CONICET, PIP 0490 and SECyT-UNCuyo 06/C456. We gratefully acknowledge the Institut Laüe Langevin (ILL) (Grenoble, France) for access to D1B, D2B and D20 powder diffractometers. F. P. thanks CONICET for a fellowship.

References

[1] P.M. Raccah, J.B. Goodenough, First-Order localized-Electron ⇆ collective-Electron transition in $LaCoO_3$, Phys. Rev. 155 (1967) 932.
[2] J.Q. Yan, J.S. Zhou, J.B. Goodenough, Ferromagnetism in $LaCoO_3$, Phys. Rev. B 70 (2004) 14402.
[3] S. Yamaguchi, Y. Okimoto, H. Taniguchi, Y. Tokura, Spin-state transition and high-spin polarons in $LaCoO_3$, Phys. Rev. B 53 (1996) R2926.
[4] M. Abbate, J.C. Fuggle, A. Fujimori, L.H. Tjeng, C.T. Chen, R. Potze, G.A. Sawatzky, H. Eisaki, S. Uchida, Electronic structure and spin-state transition of $LaCoO_3$, Phys. Rev. B 47 (1993) 16124.
[5] K. Asai, A. Yoneda, O. Yokokura, J.M. Tranquada, G. Shirane, K. Kohn, Two spin-state transitions in $LaCoO_3$, J. Phys. Soc. Japan 67 (1998) 290.
[6] S. Stølen, F. Grønvold, H. Brinks, T. Atake, H. Mori, Energetics of the spin transition in $LaCoO_3$, Phys. Rev. B 55 (1997) 14106.
[7] G. Demazeau, M. Pouchard, P. Hagenmuller, Sur de nouveaux composés oxygénés du cobalt +III dérivés de la perovskite, J. Solid State Chem. 9 (1974) 202.
[8] X. Liu, C.T. Prewitt, High-temperature diffraction study of $LnCoO_3$ perovskites: a high-order electronic phase transition, J. Phys. Chem. Solids 52 (1991) 441.
[9] S. Yamaguchi, Y. Okimoto, Y. Tokura, Bandwidth dependence of insulator-metal transitions in perovskite cobalt oxides, Phys. Rev. B 54 (1996) R11022.
[10] C. Zobel, M. Kriener, D. Bruns, J. Baier, M. Gruninger, T. Lorenz, P. Reutler, A. Revcolevschi, Evidence for a low-spin to intermediate-spin state transition in $LaCoO_3$, Phys. Rev. B 66 (2002) 020402(R).
[11] J. Baier, S. Jodlauk, M. Kriener, A. Reichl, C. Zobel, H. Kierspel, A. Freimuth, T. Lorenz, Spin-state transition and metal-insulator transition in $La_{1-x}Eu_xCoO_3$, Phys. Rev. B 71 (2005) 14443.
[12] K. Knížek, Z. Jirák, J. Hejtmánek, M. Veverka, M. Maryško, G. Maris, T.T.M. Palstra, Structural anomalies associated with the electronic and spin transitions in $LnCoO_3$, Eur. Phys. J. B 47 (2005) 213.
[13] I.A. Nekrasov, S.V. Streltsov, M.A. Korotin, V.I. Anisimov, Influence of rare-earth ion radii on the low-spin to intermediate-spin state transition in lanthanide cobaltite perovskites: $LaCoO_3$ versus $HoCoO_3$, Phys. Rev. B 68 (2003) 235113.
[14] J. Hejtmánek, Z. Jirák, K. Knı'žek, M. Maryško, M. Veverka, H. Fujishiro, Magnetism, structure and transport of $Y_{1-x}Ca_xCoO_3$ and $La_{1-x}Ba_xCoO_3$, J. Magn. Magn. Mater. 272 (2004) E283.
[15] T. Kyômen, R. Yamazaki, M. Itoh, Valence and spin state of Co and Ni ions and their relation to metallicity and ferromagnetism in $LaCo_{0.5}Ni_{0.5}O_3$, Phys. Rev. B 68 (2003) 104416.
[16] T. Moriya, New mechanism of anisotropic superexchange interaction, Phys. Rev. Lett. 4 (1960) 228.
[17] J.H. Lee, Y.K. Jeong, J.H. Park, M.A. Oak, H.M. Jang, J.Y. Son, J.F. Scott, Spin-canting-induced improper ferroelectricity and spontaneous magnetization reversal in $SmFeO_3$, Phys. Rev. Lett. 107 (2011) 117201.
[18] M. Shang, C. Zhang, T. Zhang, L. Yuan, L. Ge, H. Yuan, S. Feng, The multiferroic perovskite $YFeO_3$, Appl. Phys. Lett. 102 (2013) 62903.
[19] B. Rajeswaran, P. Mandal, R. Saha, E. Suard, A. Sundaresan, C.N.R. Rao, Ferroelectricity induced by cations of nonequivalent spins disordered in the weakly ferromagnetic perovskites $YCr_{1-x}M_xO_3$ (M = Fe or Mn), Chem. Mater. 24 (2012) 3591.
[20] E. Traversa, P. Nunziante, M. Sakamoto, Y. Sadaoka, R. Montanari, Synthesis and structural characterization of trimetallic perovskite-type oxides,;1; $LaFe_xCo_{1-x}O_3$, by the thermal decomposition of cyano complexes, $La[Fe_xCo_{1-x}(CN)_6]\cdot nH_2O$, Mater. Res. Bull. 33 (1998) 673.
[21] D.M. Gil, J. Guimpel, A. Paesano, R.E. Carbonio, M.I. Gómez, $Y[Fe_{1-x}Co_x(CN)_6]\cdot 4H_2O$ ($0 \leq x \leq 1$) solid solutions: Synthesis, crystal structure, thermal decomposition and spectroscopic and magnetic properties, J. Mol. Struct. 1015 (2012) 112.
[22] H.M. Rietveld, A Profile refinement method for nuclear and magnetic structures, J. Appl. Crystallogr. 2 (1969) 65.
[23] J. Rodríguez-Carvajal, Recent advances in magnetic structure determination by neutron powder diffraction, Phys. B Condens. Matter 192 (1993) 55.

[24] S. Mathur, M. Veith, R. Rapalaviciute, H. Shen, G.F. Goya, W.L.M. Filho, T.S. Berquo, Molecule derived synthesis of nanocrystalline $YFeO_3$ and investigations on its weak ferromagnetic behavior, Chem. Mater. 16 (2004) 1906.
[25] D.M. Gil, M.C. Navarro, M.C. Lagarrigue, J. Guimpel, R.E. Carbonio, M.I. Gómez, Crystal structure refinement, spectroscopic study and magnetic properties of yttrium hexacyanoferrate (III), J. Mol. Struct. 1003 (2011) 129.
[26] K. Knížek, Z. Jirák, J. Hejtmánek, M. Veverka, M. Maryško, B. Hauback, H. Fjellvåg, Structure and physical properties of $YCoO_3$ at temperatures up to 1000 K, Phys. Rev. B 73 (2006) 214443.
[27] R.D. Shannon, Revised effective ionic radii and systematic studies of interatomic distances in halides and chalcogenides, Acta Crystallogr. Sect. A 32 (1976) 751.
[28] P.G. Radaelli, S.-W. Cheong, Structural phenomena associated with the spin-state transition in $LaCoO_3$, Phys. Rev. B 66 (2002) 94408.
[29] E.J.J. Mallmann, A.S.B. Sombra, J.C. Goes, P.B.A. Fechine, Yttrium iron garnet: properties and applications review, Solid State Phenom. 202 (2013) 65.
[30] Y. Wei, H. Gui, Z. Zhao, J. Li, Y. Liu, S. Xin, X. Li, W. Xie, Structure and magnetic properties of the perovskite $YCo_{0.5}Fe_{0.5}O_3$, AIP Adv. 4 (2014) 127134.
[31] A.M. Are'valo-Lo'pez, M.A. Alario-Franco, Structural percolation in the $PbM_{1-x}M'_xO_3$ (M, M' = 'Ti, Cr and V) perovskites, Inorg. Chem. 50 (2011) 7136.
[32] A.A. Belik, Magnetic properties of solid solutions between $BiCrO_3$ and $BiGaO_3$ with perovskite structures, Sci. Technol. Adv. Mater. 16 (2015) 26003.
[33] J. Mao, Y. Sui, X. Zhang, Y. Su, X. Wang, Z. Liu, Y. Wang, R. Zhu, Y. Wang, W. Liu, J. Tang, Temperature- and magnetic-field-induced magnetization reversal in perovskite $YFe_{0.5}Cr_{0.5}O_3$, Appl. Phys. Lett. 98 (2011) 192510.
[34] Y. Su, J. Zhang, Z. Feng, L. Li, B. Li, Y. Zhou, Z. Chen, S. Cao, Magnetization reversal and Yb^{3+}/Cr^{3+} spin ordering at low temperature for perovskite $YbCrO_3$ chromites, J. Appl. Phys. 108 (2010) 13905.
[35] K. Hayashi, K. Ono, H. Suzuki, M. Sawada, M. Moriya, W. Sakamoto, T. Yogo, One-pot biofunctionalization of magnetic nanoparticles via thiol-ene click reaction for magnetic hyperthermia and magnetic resonance imaging, Chem. Mater. 22 (2010) 3768.
[36] M.C. Blanco, J.M. De Paoli, S. Ceppi, G. Tirao, V.M. Nassif, J. Guimpel, R.E. Carbonio, Synthesis, structural characterization and magnetic properties of the monoclinic ordered double perovskites $BaLaMSbO_6$, with M = Mn, Co and Ni, J. Alloys Compd. 606 (2014) 139.
[37] M.C. Viola, J.A. Alonso, J.C. Pedregosa, R.E. Carbonio, Crystal structure and magnetism of the double perovskite $Sr_3Fe_2MoO_9$: a neutron diffraction study, Eur. J. Inorg. Chem. 2005 (2005) 1559.
[38] E.F. Bertaut, Representation analysis of magnetic structures acta crystallogr. sect. a cryst. physics, diffraction, Theor. Gen. Crystallogr. 24 (1968) 217.
[39] P. Mandal, C.R. Serrao, E. Suard, V. Caignaert, B. Raveau, A. Sundaresan, C.N.R. Rao, Spin reorientation and magnetization reversal in the perovskite oxides $YFe_{1-x}Mn_xO_3$ ($0 < x < 0.45$): A neutron diffraction study, J. Solid State Chem. 197 (2013) 408.
[40] F. Pomiro, R.D. Sánchez, G. Cuello, A. Maignan, C. Martin, R.E. Carbonio, Spin reorientation, magnetization reversal, and negative thermal expansion observed in $RFe_{0.5}Cr_{0.5}O_3$ perovskites (R = Lu,Yb,Tm), Phys. Rev. B 94 (2016) 134402.